This article has been accepted for publication in IEEE Transactions on Neural Systems and Rehabilitation Engineering. This is the author's version which has not been fully edited and content may change prior to final publication. Citation information: DOI 10.1109/TNSRE.2022.3188184

Detection of Stroke-Induced Visual Neglect and Target Response Prediction Using Augmented Reality and Electroencephalography

Jennifer Mak*, Deniz Kocanaogullari*, Xiaofei Huang*, Jessica Kersey, Minmei Shih, Emily Grattan, Elizabeth Skidmore, George F. Wittenberg, Sarah Ostadabbas, Murat Akcakaya

***Abstract*—We aim to build a system incorporating electroencephalography (EEG) and augmented reality (AR) that is capable of identifying the presence of visual spatial neglect (SN) and mapping the estimated neglected visual field. An EEG-based brain-computer interface (BCI) was used to identify those spatiospectral features that best detect participants with SN among stroke survivors using their EEG responses to ipsilesional and contralesional visual stimuli. Frontal-central delta and alpha, frontal-parietal theta, Fp1 beta, and left frontal gamma were found to be important features for neglect detection. Additionally, temporal analysis of the responses shows that the proposed model is accurate in detecting potentially neglected targets. These targets were predicted using common spatial patterns as the feature extraction algorithm and regularized discriminant analysis combined with kernel density estimation for classification. With our preliminary results, our system shows promise for reliably detecting the presence of SN and predicting visual target responses in stroke patients with SN.**

***Index Terms*—spatial neglect, stroke, augmented reality, EEG, machine learning**

I. INTRODUCTION

VISUAL spatial neglect (SN) is a syndrome characterized by inattention to contralesional stimuli after stroke [1]. Stroke patients with SN usually display inattention to one side of themselves or the environment, neglecting to shave one side of the face or dress one side of the body. SN is heavily associated with intrahemispheric disconnections of the white matter attention networks, specifically in the frontal-parietal superior longitudinal fasciculus, and some association with interhemispheric disconnections as well [2]–[5]. Some research has also correlated lesions in the ventral frontal lobe, right inferior parietal lobe or superior temporal lobe to the manifestation of SN [6], [7]. Left-sided SN following damage to the right hemisphere (with neglect in 26.2% of stroke cases) is most common and more severe, compared to right-sided SN (in 2.4% of stroke cases) [1]. This is most likely due to the lateralization of bilateral attention processing domains to the right hemisphere of the brain [8], [9]. A diagnosis of SN is associated with extended hospitalization [10], an increased risk of falling [11], and overall poor functional recovery [12]. Current assessments of SN are insufficient to fully identify and measure the syndrome. Here, we discuss the recent developments in such assessments and present the preliminary results to our approach.

A. Related Work

The gold standard for SN assessment is the Behavioral Inattention Test (BIT). The Conventional BIT (BIT-C) consists of 6 pen-and-paper tests (line crossing, star cancellation, letter cancellation, figure and shape copying, line bisection, and representational drawing) [13]. While it is a simple and inexpensive assessment, the test is limited in its ability to account for compensatory head or body movements that patients may have developed post-stroke to adapt to their condition, such as turning the body or tilting the head to see their screens. Some subtests, like the representational drawing, may also be subjectively scored. While quantitative scores are given for each subtest, the ultimate outcome is pass/fail, rather than a grading indicating the severity of neglect. These tests also do not assess patients in a realistic and dynamic environment.

Many developments in improving the efficacy of classic pen-and-paper tests have investigated computerized methods of assessing SN. Computer-based methods have been shown to be more sensitive in detecting the presence of SN than the BIT-C [14]. Reaction time has been shown to be a reliable assessor of SN in these methods and slower reaction times are correlated with impairments to the frontal-parietal attentional networks in SN patients [15]. The Starry Night Test was successful in detecting SN in putative recovered patients, as previously determined in the BIT-C, using reaction times to visual targets among distractors [16]. The reaction times from

Jennifer Mak is with the Rehab Neural Engineering Labs and Department of Bioengineering, University of Pittsburgh, 3700 O'Hara St, Pittsburgh, PA 15213, USA. email: jem356@pitt.edu

Deniz Kocanaogullari and Murat Akcakaya are with the Department of Electrical and Computer Engineering, University of Pittsburgh, 3700 O'Hara St, Pittsburgh, PA 15213, USA. emails: dek107@pitt.edu and akcakaya@pitt.edu

Xiaofei Huang and Sarah Ostadabbas are with the Department of Electrical and Computer Engineering, Northeastern University, 360 Huntington Ave, Boston, MA 02115, USA. emails: xhuang@ece.neu.edu and ostadabbas@ece.neu.edu

Jessica Kersey is with the Department of Occupational Therapy, University of Illinois Chicago, 1919 West Taylor St., 306 AHSB., Chicago, IL 60612, USA. email: jmkersey@uic.edu

Minmei Shih, Emily Grattan, and Elizabeth Skidmore are with the Department of Occupational Therapy, University of Pittsburgh, 100 Technology Drive, Suite 350, Pittsburgh, PA 15219, USA. emails: jmk286@pitt.edu, mis235@pitt.edu, esg39@pitt.edu, skidmore@pitt.edu

George Wittenberg is with the Rehab Neural Engineering Labs and Department of Neurology, University of Pittsburgh, 3471 Fifth Avenue LKB 811, Pittsburgh, PA 15213, USA. email: geowitt@pitt.edu

This work was supported by NSF Awards #1915083 and #1915065.

*These authors contributed equally to this work.

This work is licensed under a Creative Commons Attribution-NonCommercial-NoDerivatives 4.0 License. For more information, see https://creativecommons.org/licenses/by-nc-nd/4.0/

This article has been accepted for publication in IEEE Transactions on Neural Systems and Rehabilitation Engineering. This is the author's version which has not been fully edited and content may change prior to final publication. Citation information: DOI 10.1109/TNSRE.2022.3188184

a computerized version of the classic Posner cueing test has also been used to screen for even subtle SN [17]. However, these studies still lack a method to counteract compensatory strategies, do not estimate the field of view (FOV), and produce only a binary detection result.

More recent computerized methods have used virtual reality (VR) strategies to detect SN. The Virtual Reality Lateralized Attention Test employs an obstacle-course-like paradigm with different levels of targets and unrelated background activity/distractors and participants have to name the visual targets [18]. However, these tests still only provides a binary result of neglect/no neglect. VR has also been used to quantify the volume of neglected space to determine the extent of neglect [19], but this study did not include the use of distractors. In reality, patients are often in dynamic backgrounds where many environmental distractions compete for attention, making it more difficult to isolate targets. Some patients with SN have demonstrated a reduced ability to inhibit distractors [20]–[22]. Therefore, an SN assessment tool that includes distractions amongst stimuli might better evaluate attention.

While VR may be advantageous in assessing neglect, these tools may be difficult to use for rehabilitation as the patient cannot see the real world while practicing their activities of daily living (ADLs). In examining efforts to use VR in stroke rehabilitation, it remains uncertain whether learning in a completely immersive virtual environment necessarily translates to learning in a real environment [23]. Additionally, the immersion has also been commonly reported to elicit motion sickness which could be due to a number of factors including duration of use, user health, and prior experience with VR [24]. As an alternative, augmented reality (AR) may be more suited for a rehabilitation setting as patients can still see their environment while tasks or alerts appear in their visual field in an overlay fashion. This makes the environment more comfortable and intuitive to control than an entirely virtual space, which may improve the transfer of learning and acceptance of the technology [25]. AR technologies in the past few years have been employed in medical training and condition diagnoses [26], [27] as well as in conjunction with brain-computer interfaces (BCIs) [28], [29], however, AR has not been implemented for SN evaluation or rehabilitation thus far.

In more general studies on visual attention, functional magnetic resonance imaging (fMRI) has been a common modality used to examine the functional neural correlates of visual attention. One fMRI study found distinct brain activation patterns in healthy participants performing a line bisection task [30]. Lateralization of activation to the right hemisphere was seen in the fMRI blood-oxygen-level-dependent (BOLD) response when a visual stimulus was shown [31]. Variations in the BOLD signal also differentiated between responses to valid and invalid targets during a modified a Posner task [32]. While fMRI is a non-invasive imaging technique with high spatial resolution, it has low temporal resolution and general implementation issues.

Electroencephalography (EEG) is also a non-invasive brain imaging method, but has very high temporal resolution and is relatively inexpensive to use. Time-domain analysis is useful in terms of analyzing EEG data and deep learning methodologies have been used for EEG classification. Certain EEG features were shown to be associated with SN: (i) on average there is an increase in N100 and P200 responses in the EEG of perceived targets compared to neglected targets in stroke patients, (ii) the N100a EEG component, which is expected around 130-160ms after a stimulus, does not exist in the EEG of neglect patients in response to contralesional stimuli [33] and, (iii) subcomponents of the P300 event involved in novelty stimuli detection, P3a and P3b, were reduced in amplitude towards contralesional targets in patients with SN compared to without SN [34]. Even very small visual stimuli are able to elicit measurable event-related potentials in EEG that are able to control a BCI [35]. Bandpower analysis is a useful method for analyzing EEG data in the spectral domain that calculates the average contribution of five frequency bands, including delta (0-4Hz), theta (4-8Hz), alpha (8-13Hz), beta (13-30Hz), and gamma (30-45Hz) bands to the power of the overall signal. Directing attention to external visual stimuli has been correlated with a decrease in alpha power, particularly in the parieto-occipital areas [36]. A study of non-stroke participants found an increase in alpha power in the parieto-occipital space contralateral to unattended visual stimuli [37]. After stroke, however, alpha power may fail to decrease when the eyes are open [38]. There have been few studies using bandpower analysis in stroke patients with SN. One previous study found that alpha power increased in the stroke hemisphere in patients with SN in the baseline period and during cue-orienting periods [39]. The same study showed a similar increase in stroke patients without SN but less asymmetry between hemispheres. No studies have used bandpower measures to identify SN or differentiated spectral features corresponding to fast and slow reactions to visual stimuli in stroke and stroke with SN.

B. Our Contributions

Our goal was to integrate brain imaging through EEG and AR technology in order to identify SN in stroke patients more reliably and accurately. We have developed a BCI system called AR-based EEG-guided neglect detection system called AREEN to detect SN and potentially neglected visual targets. Early and accurate neglect detection is crucial for informing rehabilitation strategies to promote functional recoveries. An ultimate goal of this project is to adapt AREEN into a multimodal system for rehabilitating acute stroke patients who present with SN. The completed system should be able to detect neglected stimuli in near real-time and alert the user to attend to the missed stimuli.

The preliminary step in AREEN system development was selecting an appropriate brain imaging modality and an AR device. We selected EEG as the measurement method in our proposed BCI system for its portability, cost-effectiveness, and high temporal resolution. For our AR system, we chose the Microsoft HoloLens, a state-of-the-art AR headset. The HoloLens enables the participant to use a Bluetooth clicker which is less constraining and easier to use than a keyboard or joystick. It will also improve on past computer-based methods by accounting for compensatory strategies. Such movements

This work is licensed under a Creative Commons Attribution-NonCommercial-NoDerivatives 4.0 License. For more information, see https://creativecommons.org/licenses/by-nc-nd/4.0/

This article has been accepted for publication in IEEE Transactions on Neural Systems and Rehabilitation Engineering. This is the author's version which has not been fully edited and content may change prior to final publication. Citation information: DOI 10.1109/TNSRE.2022.3188184

could misrepresent the number of potentially neglected targets and give a false sense of high performance. When fitted correctly, an AR headset will always center its screen in the participant's FOV; this makes our novel system more robust to compensatory techniques and FOV problems with a fixed screen.

In this paper, we illustrate the architecture of the AREEN system and propose a time synchronization method to minimize the delay due to the asynchronous signal transmission between the HoloLens and the EEG amplifier. We then evaluate the performance of the AREEN system, and present our Phase I preliminary results, starting with identifying spatiospectral features that are optimal for SN detection. Next, we develop a machine learning classification algorithm to deploy on the EEG signals to classify between potentially neglected and observed targets. This prediction can be used to estimate neglect severity in terms of the neglected visual field. We utilize multiple classifiers and specifically regularized discriminant analysis (RDA) and kernel density estimation (KDE) for classification applied on the common spatial patterns (CSP) as the extracted feature from the EEG signals. The experimental results show that our system is highly accurate in detecting neglected targets with RDA+KDE. These results will build towards the future Phase II of this study will adapt this system as a neglect rehabilitation tool that provides real-time neurofeedback.

II. METHODOLOGY

A. AR-Based EEG-Guided Neglect Detection (AREEN) System

The AREEN system is developed as an integrated multimodal tool for detection, assessment, and rehabilitation of unilateral SN caused by stroke. It detects and maps visually neglected extra-personal space with high accuracy through continuous EEG-guided SN detection. Unlike previous BCI applications which provide fixed-location visual cues, our system provides a customized application that tracks head position in real-time and projects the holographic visual cues dynamically in the participant's visual space. AREEN records EEG signals as a user views randomly appearing and disappearing targets on the AR headset display. The application itself can be considered as a cascade of multiple applications in different platforms working as a whole (Fig. 1a). A modified version of the Starry Night Test [16] is built specifically for the HoloLens in Unity Plus (Unity, San Francisco, CA, USA). The system interface is built on MATLAB R2015a and the EEG collection module is built on MATLAB R2015a with gTec MATLAB API. The computer and the Microsoft HoloLens application are connected via Bluetooth Low Energy (BLE) connection with an Arduino kit. The test is displayed on the transparent lenses where the targets and distractors are clearly seen without much obstruction to the user's vision.

B. Time synchronization of AREEN

In order to more accurately segment the EEG signal sequence, when the target appears in the HoloLens head-mounted display, a personal computer (PC) controls and sends triggers to the HoloLens to present targets and to the EEG amplifier to mark the EEG sequence being received at the same time. However, there is difference in latency between when the wireless HoloLens and wired amplifier receive the triggers (wireless technologies have higher latency). Therefore, considering this inevitable transmission delay, we use a time correction algorithm to correct the timestamp of the EEG signal marker before data analysis.

The HoloLens currently only supports two wireless data transmission modes: WiFi and Bluetooth. To minimize the wireless transmission delay, we tested the performance of both modes of transmission 1000 times in different environments (i.e. a public laboratory room, an open office area, and private home). The latency of a communications network is defined as the time needed to transport information from a sender to a receiver. One of the most commonly used measures of latency is the Round-Trip-Time (RTT), meaning the time for a packet of information to travel from the sender to the receiver and back again. Fitting the HoloLens' data transmission latencies to a beta distribution, we observe that the WiFi network is greatly affected by the environment with a very large range of transmission delay (from about 20ms to 550ms), while the Bluetooth transmission method resulted in the lesser delay time (the average of two-way delay is about 75ms), allowing for more stable communication between HoloLens and PC.

To minimize the impact of asynchronous trigger transmission, we used an offline correction method to correct each trial's EEG marker (Fig. 1c), which contains two stages: *Clock Synchronization* and k^{th} *Trial Transmission*.

In first stage, we synchronize the clocks of PC, Arduino, and HoloLens by sending the PC's time to HoloLens through an Arduino device. PC's time is defined as universal/reference time. The receipt timestamps of the Arduino and HoloLens based on universal time are noted as T_{A0} and T_H respectively. The original time of HoloLens is defined as T_O. PC first sends its timestamp T_{P0} to the Arduino. Once it receives the PC's time, the Arduino sends the current timestamp T_{A0} to the HoloLens. As soon as the HoloLens receives T_{A0}, the HoloLens will modify its own time from T_O to T_H. We note the transmission delay from PC to Arduino as D_A and assume the transmission delay between Arduino and HoloLens is constant D_m (the estimated average two-way delay divided by two) at this stage. So, the time relationships between PC and Arduino, Arduino and HoloLens can be written as:

$$T_{A0} = T_{P0} + D_A \tag{1}$$

$$T_H = T_{A0} + D_m \tag{2}$$

After synchronizing the clock (from the green dotted line in Fig. 1c), the clock of the PC, Arduino, and HoloLens shares the same time ($T_H = T_A = T_P$). The offset between the HoloLens's original time and PC's time (universal time), noted θ, can be computed:

$$\theta = T_H - T_O = T_{A0} + D_m - T_O. \tag{3}$$

For stage two, we initiate target triggers. The PC first sends the trigger to the Arduino. Once the Arduino receives the trigger, it records the timestamp and sends the trigger to the

This work is licensed under a Creative Commons Attribution-NonCommercial-NoDerivatives 4.0 License. For more information, see https://creativecommons.org/licenses/by-nc-nd/4.0/

This article has been accepted for publication in IEEE Transactions on Neural Systems and Rehabilitation Engineering. This is the author's version which has not been fully edited and content may change prior to final publication. Citation information: DOI 10.1109/TNSRE.2022.3188184

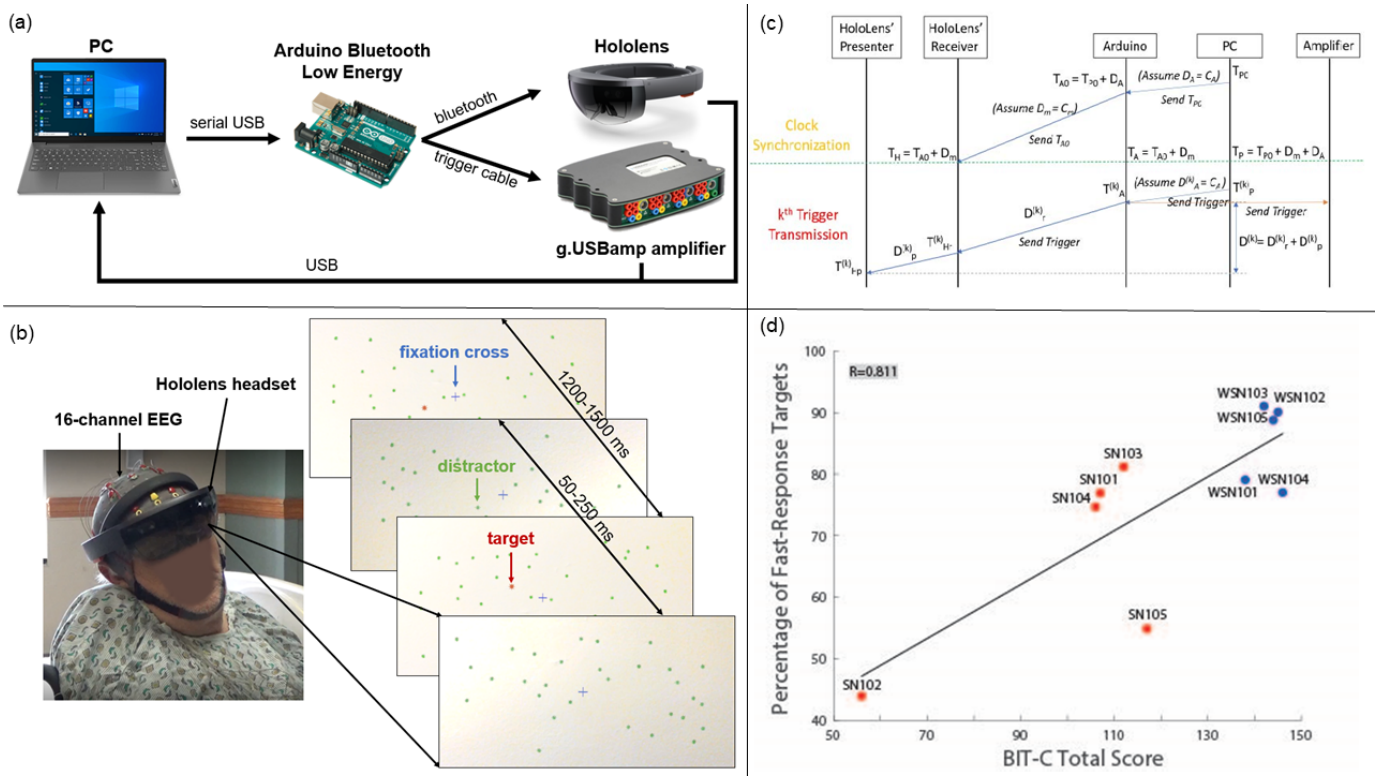

Fig. 1. (a) Flowchart that represents connections within AREEN system. PC is the main interactive terminal and control unit to activate external devices. HoloLens headset is responsible for displaying the Starry Night paradigm. g.USBamp is a high-performance biosignal amplifier for the EEG data acquisition. The ArduinoBLE module serves as a bridge to assist the PC to transmit triggers to Hololens over Bluetooth and to amplifier over cable. (b) Participant using the AREEN system, which presents the Starry Night Test paradigm. EEG electrodes are connected to the system for data collection. (c) The scheme of trigger transmission consists of two stages: Clock Synchronization and k^{th} Trial Transmission. (d) Scatter plot of participant target detection performance vs BIT-C score with a linear line of best fit and correlation coefficient R. The SN group is indicated in red and the WSN group is indicated in blue.

HoloLens and amplifier. Based on the universal time, the exact delay for each trial could be easily calculated. For the k^{th} trial, we define that PC's timestamp of sending is T_P^k, Arduino's timestamps of receiving/sending is T_A^k, the HoloLens receives the trigger at time $T_{Hr}^{(k)}$ and presents the target at time $T_{Hp}^{(k)}$. Then Arduino's sending time can be computed as:

$$T_A^{(k)} = T_P^k + D_A^k, \tag{4}$$

where D_A^k is the corresponding transmission delay from PC to Arduino for the k^{th} trial.

And the total delay between the Arduino and target presentation on HoloLens is:

$$D^{(k)} = D_p^{(k)} + D_r^{(k)} = T_{Hp}^{(k)} - T_A^{(k)}, \tag{5}$$

where $D_p^{(k)}$ and $D_r^{(k)}$ represent presentation delay and propagation delay respectively.

Since the offset θ is known in (3), the synchronized HoloLens's presentation time $T_{Hp}^{(k)}$ can be written:

$$T_{Hp}^{(k)} = T_O^{(k)} + \theta = T_O^{(k)} + T_{A0} + D_m - T_O, \tag{6}$$

where $T_O^{(k)}$ is the original HoloLens's time for the k^{th} trial.

According to (4) and (6), we can rewrite (5):

$$\begin{aligned} D^k &= T_O^k + T_{P0} + D_A + D_m - T_O - (T_P^k + D_A^k) \\ &= D_m + (T_O^k - T_O) - (T_P^k - T_{P0}) + (D_A - D_A^k). \end{aligned} \tag{7}$$

As the connections between PC and Arduino and Arduino and amplifier are wired, we assume their transmission delays are negligible ($D_A = D_A^k \approx 0$). Therefore, based on (7), only the HoloLens's elapsed time from it receiving the synchronization message to when it presents k^{th} the target, the PC's elapsed time from sending synchronization message to sending the k^{th} trigger, and the initial delay D_m need to be recorded to compute k^{th} trial delay. After data collection, the trigger markers for each trial can be shifted by transforming the delay D^k to sample points:

$$N = \left(D_m + (T_O^k - T_O) - (T_P^k - T_{P0})\right) \times \frac{F_s}{1000}, \tag{8}$$

where F_s is sampling rate 256Hz for our system setting, D_m is 37.5ms, the average two-way delay, which is estimated by testing and statistically analyzing, divided by two.

C. Participants

226 stroke patients were screened from the community and a University of Pittsburgh Medical Center inpatient rehabilitation facility. Exclusion criteria included severe visual field deficits or cognitive impairments. Participants had at least one stroke, had normal or corrected-to-normal vision, and were over 18 years old. Participants completed the BIT-C. If any BIT-C subtests scores were below each subtest's cutoff or the total score was below 129, the participant was categorized as SN. We recruited five participants with stroke

This work is licensed under a Creative Commons Attribution-NonCommercial-NoDerivatives 4.0 License. For more information, see https://creativecommons.org/licenses/by-nc-nd/4.0/

This article has been accepted for publication in IEEE Transactions on Neural Systems and Rehabilitation Engineering. This is the author's version which has not been fully edited and content may change prior to final publication. Citation information: DOI 10.1109/TNSRE.2022.3188184

and SN and five participants with stroke without SN (WSN) who completed informed consent procedures under University of Pittsburgh Institutional Review Board protocol number STUDY19060390 (approved October 8, 2019) (Table I). Each participant attended two sessions. One session from SN103 was excluded from analysis due to poor adherence to the task.

TABLE I
PARTICIPANT CHARACTERISTICS

ID	Age	Sex	Stroke Hemisphere	Days Since Stroke	BIT-C Total	BIT-C subtests at or below cutoff (/6)
SN101	81	F	Right	701	107	3
SN102	78	M	Right	17	56	6
SN103	50	M	Right	15	112	5
SN104	61	F	Left	9	106	5
SN105	37	F	Right	13	117	5
mean±SD	**61.4±18.6**	**-**	**-**	**151±307**	**100±25**	**5±1**
WSN101	35	M	Left	2404	138	0
WSN102	57	F	Left	2466	145	0
WSN103	80	M	Right	823	142	0
WSN104	27	M	Left	483	146	0
WSN105	73	M	Right	15	144	0
mean±SD	**54.4±23.1**	**-**	**-**	**1238±1130**	**143±3**	**0±0**

D. Data Collection

Participants were fitted with the EEG and HoloLens. EEG data was collected through 16 electrodes located at Fp1, Fp2, F3, F4, Fz, Fc1, Fc2, Cz, P1, P2, C1, C2, Cp3, Cp4, O1 and O2 according to the 10-20 system with a sampling frequency of 256Hz. A ground electrode was placed at Fpz and the reference electrode was placed on the left mastoid process.

We have defined four experimental modes: (1) Signal Check to check the quality of 16 channels' EEG signals in real time by visual inspection; (2) FOV Test, which allows the experimenter to calibrate the FOV in HoloLens including top, left, central, and right edges; (3) Clicker-Based Assessment for EEG data ground truth generation by identifying the locations in the HoloLens canvas in which stimuli is or is not responded to; and (4) EEG-Based Assessment to assess both existence and severity of neglect by analyzing the recorded participant's EEG in response to visual stimuli shown on random locations on the HoloLens canvas. Each experimental session began with a signal check to inspect signal quality and an FOV test to ensure proper mounting and positioning of the HoloLens. Participants then performed the Clicker-Based and EEG-Based assessments, taking breaks between tests as necessary. These assessments were completed with the participants facing blank white walls with external distractions minimized.

We designed a new paradigm in this new protocol: a modified Starry Night Test for the HoloLens (Fig. 1b). The canvas was 0.564m wide $\times$ 0.288m tall, divided into a 6$\times$12 grid (72 total cells) with a fixed depth of 1.14m. Only one stimulus can occupy one cell at a time. 30-35 distractors, or green stars, were shown at a time for 0.05s-0.25s across the grid. Targets, or red stars, were shown one at a time 216 times total, (three times in each cell) in a random order for a maximum of 3s during the Clicker-Based Assessment and FOV test and 0.066s in EEG-Based Assessment. Time between targets was randomized 1.2s-2.5s. Randomizing the appearance of targets and distractors reduces the risk of seizure due to rhythm photic stimulation [40]. In this study, all participants were able to distinguish between red and green stars. However, it is possible that future users may experience red-green colorblindness. The colors of these stars are easily reprogrammable in the app developer.

During the Clicker-Based Assessment, participants have up to 3s to responded to a target using the remote clicker and reaction time is collected. No EEG is collected during this period. During the EEG-Based Assessment, targets appear for a fixed time, as the participant does not give direct input to the system but their EEG is collected. The target number order is recorded for both assessments.

E. Preprocessing

The EEG data was filtered through an 8$^{\text{th}}$ order Butterworth bandpass filter (2-62 Hz) and a 4$^{\text{th}}$ order notch filter (58-62 Hz). Data samples were shifted according to the recorded transmission delay times. The data was then segmented into signal and baseline segments, or 500ms following and 200ms prior the appearance of a target, respectively. The average baseline amplitude was subtracted from the signal segment in the time-domain for baseline correction. Artifact removal and repairing was completed using the Autoreject algorithm [41]. The total number of trials preserved after Autoreject and therefore used for analyses are detailed in Table I.

The 6$\times$12 display grid was divided down the middle so that half the cells are on the left and the other half are on the right. For each participant, EEG segments to the targets corresponding to the target location are labeled "ipsilesional" or "contralesional", based on the lesioned hemisphere for each participant. The EEG data was also labeled with their corresponding band and electrodes. There are a total of 80 possible labels, as there are 16 electrodes and five bands.

For each session, the median reaction times of the three responses per each of the 72 targets were thresholded using a majority-voting procedure. Getting the median increases the number of slow-response targets in a way that is more robust compared to getting the mean in terms of outlier behaviour. These times were thresholded using Otsu's method [42]. Otsu's method, while mainly used for image binarization, is an algorithm that iteratively searches for a threshold. The selected threshold maximizes the variance (equivalently minimizing the intra-class variance) between two classes: slow-response and fast-response.

For intra-class variance defined as $\sigma^2_{intra}(i) = \omega_0(i)\sigma^2_0(i) + \omega_1(i)\sigma^2_1(i)$, weights $\omega_{0,1}$ are probabilities of the classes separated by a threshold i. $\sigma^2_{0,1}$ are variances of the classes. $\omega_{0,1}(i)$ are computed from k-bin histogram:

$$\omega_0(i) = \sum_{x=0}^{i-1} p(x)$$

$$\omega_1(i) = \sum_{x=i}^{k-1} p(x)$$

For two classes, as stated above, minimizing intra-class variance is equivalent to maximizing inter-class variance:

This work is licensed under a Creative Commons Attribution-NonCommercial-NoDerivatives 4.0 License. For more information, see https://creativecommons.org/licenses/by-nc-nd/4.0/

This article has been accepted for publication in IEEE Transactions on Neural Systems and Rehabilitation Engineering. This is the author's version which has not been fully edited and content may change prior to final publication. Citation information: DOI 10.1109/TNSRE.2022.3188184

$$\sigma_b^2(i) = \sigma^2 - \sigma_w^2(i) = \omega_0(i)(\mu_0 - \mu_T)^2 + \omega_1(i)(\mu_1 - \mu_T)^2 = \omega_0(i)\omega_1(i)\left[\mu_0(i) - \mu_1(i)\right]^2$$

where $\omega_{0,1}$ are class probabilities, $\mu_{0,1}$ are class means and μ_T is given by:

$$\omega_0\mu_0 + \omega_1\mu_1 = \mu_T \tag{9}$$

Reaction times above the threshold were labeled as slow responses. Reaction times below the threshold were labeled as fast responses. The fast and slow labels are meant to characterize response segments as high attention and low attention states, respectively.

F. Neglect Detection

Bandpowers for delta (0-4 Hz), theta (5-8 Hz), alpha (9-13 Hz), beta (14-30 Hz), and gamma (31-45 Hz) bands were calculated for each signal and baseline segment at each electrode channel. The powers of the ipsilesional responses and contralesional responses were combined from all the participants in this analysis. At each electrode-band location, a power ratio was calculated such that each ipsilesional-response power was divided by the average contralesional-response power. The log of these ratios was taken for analyses. This ratio represents neural activation in the ipsilesional response normalized with respect to the average contralesional response. Wilcoxon rank sum tests with Bonferroni-correction were conducted for every electrode within each band to find significant differences in power ratios (*n*=940 in WSN, *n*=852 in SN) between the two groups. A logistic regression analysis was performed using the significant electrode-band locations as features to evaluate the ability of these power ratios to separate SN from WSN. Results were validated with 10-fold cross validation with random shuffling.

G. Response Prediction

A machine-learning based classification algorithm was created to distinguish between slow-response and fast-response targets across SN and WSN participants. We have applied multiple classifiers that are used in EEG analysis: Quadratic and Linear Discriminant Analyses (QDA and LDA) [43], AdaBoost [44], Random Forest Classifier (RFC) [45], Naive Bayes [46], Multilayer Perceptron (MLP) [47], Regularized Discriminant Analysis and Kernel Density Estimation (RDA+KDE) [48]. RDA+KDE is the main classifier that we have worked on and has been demonstrated to work well on event-related potentials (ERP). [49], whereas the other classifiers are used for comparison. However, here we use a different feature extraction method than channel-wise principal component analysis approach, which is used in [48]. We are using common spatial patterns (CSP) as the feature extraction algorithm.

1) Common Spatial Patterns as Discriminative Features: Common spatial patterns (CSP) is an algorithm to calculate spatial filters and it is widely used in BCI systems. It was first proposed to classify imagined hand movements by using multi-channel EEG [50]. The goal is to design a pair of spatial filters such that the filtered signal's variance is maximal for one class while minimal for the other, and vice versa.

Let $X_i \in \mathbb{R}^{N_i \times C}$ be the filtered EEG signals, where $i \in 1, 2$ denotes the class. The algorithm computes a spatial filter $w \in \mathbb{R}^C$

$$\max_{\mathbf{w}} \frac{w^T X_1^T X_1 w}{w^T X_2^T X_2 w} \tag{10}$$

As the equation above is invariant with the scale of $w, \forall w \neq 0$, it can be formulated as

$$\max_{\mathbf{w}} w^T X_1^T X_1 w \;\text{ s.t. }\; w^T X_2^T X_2 w = 1 \tag{11}$$

Finally, by applying Lagrange multiplier, this results in the generalized eigenvalue problem

$$X_1^T X_1 w = \lambda X_2^T X_2 w \tag{12}$$

To find multiple spatial filters W, solving the simultaneous diagonalization problem

$$\max_{\mathbf{W} \in \mathbb{R}^{\mathbf{C} \times \mathbf{K}}} \text{trace}(\Lambda)$$
$$\text{s.t. } W^T X_1^T X_1 W = \Lambda,\; W^T X_2^T X_2 W = I$$

where K is the number of spatial filters, Λ is a diagonal matrix of shape $K \times K$, and I is the identity matrix

After taking 16 vectors from each trial using CSP, the average power of each vector is extracted and classified.

With **X** being a normal distributed variable, the classification rule can be given as

$$d_{\hat{k}}(\mathbf{X}) = \min_{1 \leq k \leq K} d_k(\mathbf{X}) \tag{13}$$

with

$$d_k(\boldsymbol{X}) = (\boldsymbol{X} - \boldsymbol{\mu_k})^T \Sigma_k^{-1} (\boldsymbol{X} - \boldsymbol{\mu_k}) + ln|\Sigma_k| - 2ln\pi_k \tag{14}$$

where $\boldsymbol{\mu_k}$ and Σ_k are class mean vector and covariance matrix respectively and π_k is the unconditional prior probability of observing a class *k* data. Equation 14 is called the discriminant score for *k*th class. Using equations 13 and 14 results in using quadratic discriminant analysis (QDA) for classification. If class covariance matrices are assumed identical, i.e. $\Sigma_k = \Sigma, 1 \leq k \leq K$ it results in linear discriminant analysis (LDA). When class sample sizes N_k are smaller compared to the dimension of the measurement space p, covariance matrix estimates get highly variable. Regularized discriminant analysis (RDA) [51] attempts to overcome this problem by introducing two parameters for estimating the class covariance matrices: λ and γ. λ is used for regularization of individual class covariance matrices towards a pooled estimate. $\lambda = 0$ results in LDA whereas $\lambda = 1$ results in QDA. γ shrinks those class covariance matrices towards a multiple of identity matrix. This parameter is used to alleviate the effects of eigenvalue bias: it decreases the larger eigenvalues and increases the smaller ones. The equation wholly becomes:

$$\hat{\Sigma}_k(\lambda, \gamma) = (1 - \gamma)\hat{\Sigma}_k(\lambda) + \frac{\gamma}{p} tr[\hat{\Sigma}_k(\lambda)]I \tag{15}$$

RDA is the main classifier scope of this paper and the calculations are performed on the data from CSP. After getting

This work is licensed under a Creative Commons Attribution-NonCommercial-NoDerivatives 4.0 License. For more information, see https://creativecommons.org/licenses/by-nc-nd/4.0/

This article has been accepted for publication in IEEE Transactions on Neural Systems and Rehabilitation Engineering. This is the author's version which has not been fully edited and content may change prior to final publication. Citation information: DOI 10.1109/TNSRE.2022.3188184

scores for each datapoint from RDA, we use kernel density estimation (KDE) with a Gaussian kernel to make predictions.

The dataset is comprised of 10 participants, where each participant may have multiple experimental sessions. As there are fewer slow responses than fast responses in all participants, our dataset is imbalanced with a 1:7 ratio, which is preserved after Autoreject. We use all 16 CSP vectors' average powers as features in temporal analysis.

III. RESULTS

The estimated number of fast and slow responses thresholded from the Clicker-Based Assessment are listed for each participant in Table II. The percentage of fast responses for each participant has a positive correlation with BIT scores ($R = 0.811$), with a division in performances between SN and WSN (Fig. 1d). This demonstrates an expected aspect of AREEN system performance.

TABLE II
TARGET RESPONSE DATA

ID	Fast Responses	Slow Responses	Total Responses	Median Reaction Time (s)
SN101	260	78	338	1.42
SN102	188	240	428	2.13
SN103	164	38	202	1.06
SN104	221	75	296	1.48
SN105	237	195	432	1.73
mean±SD	**214±38**	**125±87**	**339±96**	**1.56±0.370**
WSN101	340	90	430	0.700
WSN102	363	40	403	0.892
WSN103	366	36	402	0.766
WSN104	268	80	348	0.683
WSN105	261	33	294	0.801
mean±SD	**320±27**	**56±27**	**375±54**	**0.768±0.0841**

Topographic visualizations of the power ratios reveal similar trends within the two groups' responses to targets across frequency bands, with a few differences in spatial distribution (Fig. 2a). Most noticeably, a normalized ipsilesional response within the WSN group is generally most powerful in the highest frequencies (beta and gamma); within the SN group, this is most powerful in theta and beta. In the WSN group, the occipital region is the location of highest power ratio in every band. In the SN group, the points of highest power ratio are concentrated in the central-parietal regions in the lower frequencies (delta and theta) and shifted to the frontal-central regions in the upper frequencies (alpha, beta, and gamma). Both groups see highest power ratios in beta. Between groups, SN generally has higher power ratios in theta and alpha but lower gamma than WSN. In both groups, spatial distributions of power ratio generally vary symmetrically across hemispheres.

A. Neglect Detection

The Wilcoxon rank sum tests using the power ratios found 50 statistically significant ($p<0.0006$) locations out of the 80 possible locations (Fig. 2b). These locations describe nearly the whole brain in delta, theta, and alpha except in occipital electrodes, frontal beta, and mostly left frontal-parietal gamma. These significant areas are symmetric in all bands except gamma. Additional Wilcoxon rank sum tests were performed to compare power ratios in the left and right electrodes within each group and no significant differences were found. The logistic regression analysis using the power ratios at these significant locations yielded an average area under the receiver-operator-characteristic curve (AUC) of 0.853 and 0.832 for the training and testing sets, respectively, demonstrating the high detection probability of an SN participant based on this metric. From the regression, 17 locations were significant, or important to the prediction of neglect, describing frontal-central delta and alpha, frontal-parietal theta, Fp1 beta, and left frontal gamma.

B. Response Prediction

Here, we present the results for classification between recorded EEG responses corresponding to the slow-response and fast-response targets for the SN and WSN groups to show the performance of our proposed classifier for identification of potentially neglected targets. The results in Table III are obtained through 10-fold cross validation. The results given in the table are average AUC's over folds. We also plotted two examples of the estimated neglected visual fields from participants SN102 (Fig. 3a) and SN101 (Fig. 3b), representing the varying degrees in prediction accuracy.

The results demonstrate that using RDA+KDE shows greater performance compared to other methods whereas RFC and MLP overfits. In this classifier, we only train for RDA, where all λ and γ values are searched and the pair with highest AUC is picked. After getting the 'best' λ and γ values, test data is put through RDA with best λ, γ pair and then KDE. The search for λ and γ values are done in a brute force manner, contrary to what is provided with BciPy, where 100 values between 0 and 1 are tried and train AUC are gotten for each fold. BciPy uses constrained optimization by linear approximation algorithm, also known as Powell's method [52], which does not rely on derivative calculation and -AUC was used as the loss function. We initially chose to search for all the results for our exploratory work where we checked for the impact of λ and γ values.

The temporal analysis takes both slow and fast responses from SN patients and only fast responses from WSN patients. Trials thresholded as slow responses are removed from the WSN group, as slow responses can be considered potentially neglected responses and WSN patients do not have an SN diagnosis. As Phase I is still ongoing and we will be working on SN patients only from Phase II onwards, data from WSN patients are added for data augmentation.

We have used Python for temporal analysis and the following libraries: numpy [53], scikit-learn [54], MNE [55], Autoreject [41], BciPy [48].

IV. DISCUSSION

In this study, we have shown that the AREEN system can feasibly detect SN using the spatiospectral features from EEG responses to visual targets. These features lie within all frequency bands, although there are distinct areas of activation within each band. Similar to another study using EEG and AR

This work is licensed under a Creative Commons Attribution-NonCommercial-NoDerivatives 4.0 License. For more information, see https://creativecommons.org/licenses/by-nc-nd/4.0/

This article has been accepted for publication in IEEE Transactions on Neural Systems and Rehabilitation Engineering. This is the author's version which has not been fully edited and content may change prior to final publication. Citation information: DOI 10.1109/TNSRE.2022.3188184

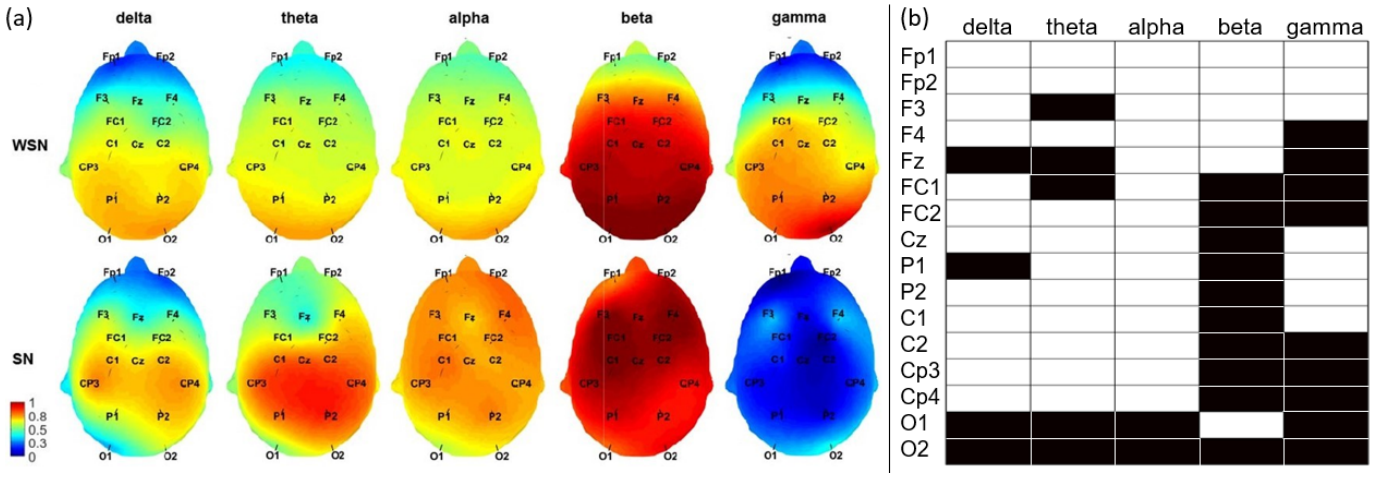

Fig. 2. (a) Topographic head plots of power ratios averaged across all trials of all participants within each group. Plots are scaled all together and normalized [0,1].(b) Results of Wilcoxon rank sum tests comparing median power ratios between WSN and SN. White spaces indicate locations that were significantly different between groups. Black spaces indicate locations that were not significantly different between groups.

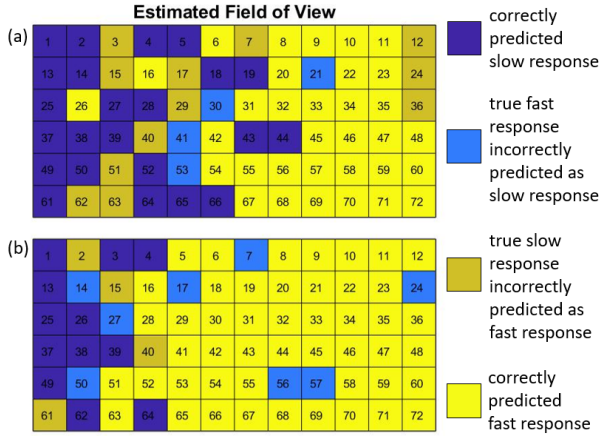

Fig. 3. The estimated FOV plots from two participants, exemplifying moderate prediction accuracy (a) and high prediction accuracy (b). The grids show the canvas with the 72 locations in which targets appear. The colors correspond to the predictions of ”fast” or ”slow” at each location.

TABLE III
CLASSIFICATION RESULTS

Method	Average Train AUC	Average Test AUC
QDA	0.728	0.698
LDA	0.636	0.629
AdaBoost	0.681	0.615
RFC	0.999	0.604
Gaussian Naive-Bayes	0.717	0.716
MLP	0.816	0.613
RDA+KDE	**0.788**	**0.760**

to classify attention [56], important features were distributed across bands and many were located in the frontal area. Diverging from those results, we found significance also within the delta band and parietal-occipital areas. Higher power in low frequencies is typically associated with decreased cognitive function and poorer stroke recovery outcomes [57]. This is consistent with the trend seen in power ratios between groups, as the SN group is considered more impaired. Frontal-parietal and parietal-occipital regions are important areas regarding visuospatial attention. Neglect pathology is heterogenous but can generally be correlated with dorsal frontal-parietal network structural or functional dysfunction [58], [59]. The condition is also related to parietal-occipital damage which plays a role in selective attention [60].

High beta and gamma activity in the left occipital area has been correlated with impaired attention selectivity [61]. From the statistical analyses, we find that the left occipital electrode, O1, had higher power ratios in beta in the SN group compared to the WSN group. However, this is the only electrode representing the entire left occipital cortex, so this outcome should be considered with caution. Frontal-central beta synchronization has also been relevant to premotor activity in neglect [62]. In our study, this may be explained by more undesired movements from the SN gropu during the EEG-Based Assessment. In addition to this, perhaps the most striking difference seen in the present study is the power ratio decrease in gamma in the SN group compared to the WSN group. The reason for this difference remains unclear as this has not been previously observed in literature.

Increased task-related alpha activity in the parietal-occipital region is thought to be related to the inhibition of external stimuli, particularly distracting or irrelevant stimuli [63], [64]. Therefore, we could expect to see high alpha power ratio from the WSN group in this region, as they should be better at inhibiting the distractor stars in the Starry Night Task. However, we actually saw greater alpha in the parietal region in the SN group compared to the WSN group and there were no significant differences from the occipital region. This suggests a more general problem at the earliest stages of attention to stimuli, salient or not. Additionally, parietal theta was also higher in the SN group. Although the theta band produced the fewest significant features for neglect detection, the presence of some significant locations in this band expands upon previous findings that did not implicate its importance in identifying post-stroke cognitive deficits [65]. Increased theta and alpha activity have been linked to greater mental fatigue [66], [67] which might account for some of the higher power in these frequencies in the SN group. Participants were encouraged to take breaks between the Clicker-Based and EEG-Based assessments, but at least one participant verbally reported feeling fatigued due to the length of the tests and

This work is licensed under a Creative Commons Attribution-NonCommercial-NoDerivatives 4.0 License. For more information, see https://creativecommons.org/licenses/by-nc-nd/4.0/

This article has been accepted for publication in IEEE Transactions on Neural Systems and Rehabilitation Engineering. This is the author's version which has not been fully edited and content may change prior to final publication. Citation information: DOI 10.1109/TNSRE.2022.3188184

the requirement to remain still and fixate. Participants in the SN group generally fatigued more and faster than those in the WSN group. This could have further impaired their performance on the task and ability to concentrate.

In this study, power ratio maps within any band tended to be symmetric. Previous research suggests that activation within hemispheres may depend on the location of the stimuli with respect to the lesioned hemisphere [37], [39], [68]. A possible explanation for the departure from the literature is the nature of our metric. The power ratio incorporates responses to both ipsilesional and contralesional targets. Additionally, we recruited both left-hemisphere and right-hemisphere damaged participants in both groups. This study did not control for stroke hemisphere, as the goal of this project was to find general spatiospectral features that would identify SN. Doing so could possibly reveal these hemispheric distribution patterns and improve classification accuracy, but the result may be that we develop a system only applicable for a subset of the neglect population. Future work could investigate using spectral metrics that are robust to inter-individual EEG differences within a group, such as individual alpha frequency, to output more relevant, precise measures for neglect detection or personalized metrics for each patient.

Compared to other related neglect detection systems [69], [70], AREEN more accurately detects the presence of neglect by evaluating its neural signatures rather than behavioral metrics. Our system also demonstrates higher accuracy in classifying potentially neglected and observed targets than a similar previously proposed system [33] and is the first to attempt to do so in neglect patients via EEG. The ultimate purpose of the classification algorithms presented in this study is to propose an initial step towards our end goal: rehabilitation. RDA+KDA, though simple compared to state-of-the-art deep learning models, has demonstrated high AUC values with 10-fold cross validation in our limited dataset. Each fold in cross-validation is stratified; each set is forced to keep the ratio of slow- and fast-response targets. Additionally, given there are five participants with SN and five without SN, one can concur that the model is generalizable. Even though the average results from 10-fold cross validation are good, future translation into rehabilitation requires a highly accurate classifier that can work in the patient's real-world environment.

Our future Phase II research will be conducted only on patients with SN. For initial analyses, leave-one-out cross-validation for SN participants will be chosen to analyze each participant by themselves: a participant is set as test set and the remainder is used for training. However, EEG data is highly variable person-to-person. While the number of participants from each group is equal, the number of potentially neglected targets are still lower than the number of potentially observed ones. Therefore, we observed an overfitting issue where the model tends to pick class 0, fast-response or potentially observed targets. Both our previous work [71] and statistical analyses reported in this paper also demonstrate that neglect detection with EEG is possible. Thus, as we collect more data and go into Phase II, we will create a multiobjective optimization algorithm for online rehabilitation utilizing a neglect detection and a neglected target detection objectives together.

This study has several limitations. More sophisticated statistical analyses may illuminate different activation patterns and spatiospectral relationships that better align with those seen in literature. However, our strategy has been used in similar EEG analyses [72], [73] and still yielded many significant features that separated the groups with high accuracy despite using a very conservative α to correct for multiple comparisons. Due to the small sample size in this study, the results of this study are only preliminary and will need to be verified with a larger cohort. The time since stroke also varied widely as this study incorporated both acute and chronic stroke participants. It is possible that there are differences in the EEG responses between the two groups, especially as the brain rapidly reorganizes in the weeks post-stroke.

Additionally, eye-tracking technology would have been beneficial to this experimental setup. The HoloLens used in this implementation (1st generation) did not have this capability, but it is offered in the 2nd generation device. For this study's setup, this addition would also verify gaze fixation at the center of the screen without verbal prompting which could introduce an external distraction and elicit an undesired EEG response. Eye-tracking would open further avenues for analyses for neglect detection as this technology has been used in previous research for such purposes [74], [75]. Gaze patterns and pupil dilations have been used to detect neglect, often with higher sensitivity than classic pen-and-paper tests [76]–[78].

V. CONCLUSIONS

In this paper, we presented our AREEN system that incorporates an augmented reality (AR) headset into a BCI framework, and developed and tested an EEG-based BCI for SN detection. It was also demonstrated that spatiospectral features for detecting SN could be identified from statistically significant power ratios. In future work, band synchronizations may be observed between regions of the brain and across hemispheres. We also extracted features using common spatial patterns and demonstrated performances of multiple classifiers to identify EEG features. We specifically used RDA+KDA to detect potentially neglected targets. This method is highly accurate in detecting neglect, as demonstrated by the high AUC. Future research will implement the proposed AREEN system in rehabilitation of patients with SN. Specifically, a real-time feedback system for patients with SN will be developed to draw their attention to neglected stimuli; visual and auditory feedback will be given to the participant by processing EEG data in real-time. The rehabilitation process will be conducted during ADLs to provide a dynamic and realistic setup for participants.

REFERENCES

[1] E. Becker and H.-O. Karnath, "Incidence of visual extinction after left versus right hemisphere stroke," Stroke, vol. 38, no. 12, pp. 3172–3174, 2007.

[2] A. Baldassarre, L. Ramsey, C. L. Hacker, A. Callejas, S. V. Astafiev, N. V. Metcalf, K. Zinn, J. Rengachary, A. Z. Snyder, A. R. Carter et al., "Large-scale changes in network interactions as a physiological signature of spatial neglect," Brain, vol. 137, no. 12, pp. 3267–3283, 2014.

This work is licensed under a Creative Commons Attribution-NonCommercial-NoDerivatives 4.0 License. For more information, see https://creativecommons.org/licenses/by-nc-nd/4.0/

This article has been accepted for publication in IEEE Transactions on Neural Systems and Rehabilitation Engineering. This is the author's version which has not been fully edited and content may change prior to final publication. Citation information: DOI 10.1109/TNSRE.2022.3188184

[3] F. Doricchi, M. T. de Schotten, F. Tomaiuolo, and P. Bartolomeo, "White matter (dis) connections and gray matter (dys) functions in visual neglect: gaining insights into the brain networks of spatial awareness," cortex, vol. 44, no. 8, pp. 983–995, 2008.

[4] P. Bartolomeo, M. Thiebaut de Schotten, and F. Doricchi, "Left unilateral neglect as a disconnection syndrome," Cerebral cortex, vol. 17, no. 11, pp. 2479–2490, 2007.

[5] B. Spanò, D. Nardo, G. Giulietti, A. Matano, I. Salsano, C. Briani, R. Vadalà, C. Marzi, M. De Luca, C. Caltagirone et al., "Left egocentric neglect in early subacute right-stroke patients is related to damage of the superior longitudinal fasciculus," Brain imaging and behavior, vol. 16, no. 1, pp. 211–218, 2022.

[6] G. Committeri, S. Pitzalis, G. Galati, F. Patria, G. Pelle, U. Sabatini, A. Castriota-Scanderbeg, L. Piccardi, C. Guariglia, and L. Pizzamiglio, "Neural bases of personal and extrapersonal neglect in humans," Brain, vol. 130, no. 2, pp. 431–441, 2007.

[7] G. Vallar and D. Perani, "The anatomy of unilateral neglect after right-hemisphere stroke lesions. a clinical/ct-scan correlation study in man," Neuropsychologia, vol. 24, no. 5, pp. 609–622, 1986.

[8] M.-M. Mesulam, "A cortical network for directed attention and unilateral neglect," Annals of Neurology: Official Journal of the American Neurological Association and the Child Neurology Society, vol. 10, no. 4, pp. 309–325, 1981.

[9] A. Dragone, S. Lasaponara, M. Silvetti, E. Macaluso, and F. Doricchi, "Selective reorienting response of the left hemisphere to invalid visual targets in the right side of space: Relevance for the spatial neglect syndrome," Cortex, vol. 65, pp. 31–35, 2015.

[10] P. Appelros, "Prediction of length of stay for stroke patients," Acta Neurologica Scandinavica, vol. 116, no. 1, pp. 15–19, 2007.

[11] P. Chen, K. Hreha, Y. Kong, and A. Barrett, "Impact of spatial neglect on stroke rehabilitation: evidence from the setting of an inpatient rehabilitation facility," Archives of physical medicine and rehabilitation, vol. 96, no. 8, pp. 1458–1466, 2015.

[12] L. J. Buxbaum, M. Ferraro, T. Veramonti, A. Farne, J. Whyte, E. Ladavas, F. Frassinetti, and H. Coslett, "Hemispatial neglect: Subtypes, neuroanatomy, and disability," Neurology, vol. 62, no. 5, pp. 749–756, 2004.

[13] B. Wilson, J. Cockburn, and P. Halligan, "Development of a behavioral test of visuospatial neglect." Archives of physical medicine and rehabilitation, vol. 68, no. 2, pp. 98–102, 1987.

[14] M. Bonato, K. Priftis, C. Umiltà, and M. Zorzi, "Computer-based attention-demanding testing unveils severe neglect in apparently intact patients," Behavioural Neurology, vol. 26, no. 3, pp. 179–181, 2013.

[15] A. Bourgeois, A. B. Chica, R. Migliaccio, M. T. de Schotten, and P. Bartolomeo, "Cortical control of inhibition of return: evidence from patients with inferior parietal damage and visual neglect," Neuropsychologia, vol. 50, no. 5, pp. 800–809, 2012.

[16] L. Y. Deouell, Y. Sacher, and N. Soroker, "Assessment of spatial attention after brain damage with a dynamic reaction time test," Journal of the International Neuropsychological Society: JINS, vol. 11, no. 6, p. 697, 2005.

[17] J. Rengachary, G. d'Avossa, A. Sapir, G. L. Shulman, and M. Corbetta, "Is the posner reaction time test more accurate than clinical tests in detecting left neglect in acute and chronic stroke?" Archives of physical medicine and rehabilitation, vol. 90, no. 12, pp. 2081–2088, 2009.

[18] L. J. Buxbaum, A. M. Dawson, and D. Linsley, "Reliability and validity of the virtual reality lateralized attention test in assessing hemispatial neglect in right-hemisphere stroke." Neuropsychology, vol. 26, no. 4, p. 430, 2012.

[19] A. Y. Dvorkin, R. A. Bogey, R. L. Harvey, and J. L. Patton, "Mapping the neglected space: gradients of detection revealed by virtual reality," Neurorehabilitation and neural repair, vol. 26, no. 2, pp. 120–131, 2012.

[20] A. Saj, V. Verdon, C.-A. Hauert, and P. Vuilleumier, "Dissociable components of spatial neglect associated with frontal and parietal lesions," Neuropsychologia, vol. 115, pp. 60–69, 2018.

[21] J. A. Cox and A. M. A. Davies, "Keeping an eye on visual search patterns in visuospatial neglect: A systematic review," Neuropsychologia, vol. 146, p. 107547, 2020.

[22] R. L. Emerson, A. García-Molina, J. L. Carballo, J. G. Fernández, C. Aparicio-López, J. Novo, R. Sánchez-Carrión, A. Enseñat-Cantallops, and J. Peña-Casanova, "Visual search in unilateral spatial neglect: The effects of distractors on a dynamic visual search task," Applied Neuropsychology: Adult, 2018.

[23] W.-S. Kim, S. Cho, J. Ku, Y. Kim, K. Lee, H.-J. Hwang, and N.-J. Paik, "Clinical application of virtual reality for upper limb motor rehabilitation in stroke: review of technologies and clinical evidence," Journal of clinical medicine, vol. 9, no. 10, p. 3369, 2020.

[24] E. Chang, H. T. Kim, and B. Yoo, "Virtual reality sickness: a review of causes and measurements," International Journal of Human–Computer Interaction, vol. 36, no. 17, pp. 1658–1682, 2020.

[25] C. Gorman and L. Gustafsson, "The use of augmented reality for rehabilitation after stroke: a narrative review," Disability and rehabilitation: assistive technology, pp. 1–9, 2020.

[26] J. Ara, H. Bhuiyan, Y. A. Bhuiyan, S. B. Bhyan, and M. I. Bhuiyan, "Ar-based modern healthcare: A review," arXiv preprint arXiv:2101.06364, 2021.

[27] J. Sutherland, J. Belec, A. Sheikh, L. Chepelev, W. Althobaity, B. J. Chow, D. Mitsouras, A. Christensen, F. J. Rybicki, and D. J. La Russa, "Applying modern virtual and augmented reality technologies to medical images and models," Journal of digital imaging, vol. 32, no. 1, pp. 38–53, 2019.

[28] A. Lenhardt and H. Ritter, "An augmented-reality based brain-computer interface for robot control," in International Conference on Neural Information Processing. Springer, 2010, pp. 58–65.

[29] J. K. Zao, T.-P. Jung, H.-M. Chang, T.-T. Gan, Y.-T. Wang, Y.-P. Lin, W.-H. Liu, G.-Y. Zheng, C.-K. Lin, C.-H. Lin et al., "Augmenting vr/ar applications with eeg/eog monitoring and oculo-vestibular recoupling," in International Conference on Augmented Cognition. Springer, 2016, pp. 121–131.

[30] G. R. Fink, J. C. Marshall, P. H. Weiss, I. Toni, and K. Zilles, "Task instructions influence the cognitive strategies involved in line bisection judgements: evidence from modulated neural mechanisms revealed by fmri," Neuropsychologia, vol. 40, no. 2, pp. 119–130, 2002.

[31] A. Hougaard, B. H. Jensen, F. M. Amin, E. Rostrup, M. B. Hoffmann, and M. Ashina, "Cerebral asymmetry of fmri-bold responses to visual stimulation," PLoS One, vol. 10, no. 5, p. e0126477, 2015.

[32] M. Silvetti, S. Lasaponara, F. Lecce, A. Dragone, E. Macaluso, and F. Doricchi, "The response of the left ventral attentional system to invalid targets and its implication for the spatial neglect syndrome: a multivariate fmri investigation," Cerebral Cortex, vol. 26, no. 12, pp. 4551–4562, 2016.

[33] A. Khalaf, J. Kersey, S. Eldeeb, G. Alankus, E. Grattan, L. Waterstram, E. Skidmore, and M. Akcakaya, "Eeg-based neglect assessment: a feasibility study," Journal of neuroscience methods, vol. 303, pp. 169–177, 2018.

[34] S. Lasaponara, M. D'Onofrio, M. Pinto, A. Dragone, D. Menicagli, D. Bueti, M. De Lucia, F. Tomaiuolo, and F. Doricchi, "Eeg correlates of preparatory orienting, contextual updating, and inhibition of sensory processing in left spatial neglect," Journal of Neuroscience, vol. 38, no. 15, pp. 3792–3808, 2018.

[35] M. Xu, X. Xiao, Y. Wang, H. Qi, T.-P. Jung, and D. Ming, "A brain–computer interface based on miniature-event-related potentials induced by very small lateral visual stimuli," IEEE Transactions on Biomedical Engineering, vol. 65, no. 5, pp. 1166–1175, 2018.

[36] E. Magosso, F. De Crescenzio, G. Ricci, S. Piastra, and M. Ursino, "Eeg alpha power is modulated by attentional changes during cognitive tasks and virtual reality immersion," Computational intelligence and neuroscience, vol. 2019, 2019.

[37] S. Kelly, E. Lalor, R. Reilly, and J. Foxe, "Independent brain computer interface control using visual spatial attention-dependent modulations of parieto-occipital alpha," in Conference Proceedings. 2nd International IEEE EMBS Conference on Neural Engineering, 2005. IEEE, 2005, pp. 667–670.

[38] M. Molnár, R. Csuhaj, S. Horváth, I. Vastagh, Z. A. Gaál, B. Czigler, A. Bálint, D. Csikós, and Z. Nagy, "Spectral and complexity features of the eeg changed by visual input in a case of subcortical stroke compared to healthy controls," Clinical neurophysiology, vol. 117, no. 4, pp. 771–780, 2006.

[39] S. Lasaponara, M. Pinto, M. Aiello, F. Tomaiuolo, and F. Doricchi, "The hemispheric distribution of α-band eeg activity during orienting of attention in patients with reduced awareness of the left side of space (spatial neglect)," Journal of Neuroscience, vol. 39, no. 22, pp. 4332–4343, 2019.

[40] R. S. Fisher, G. Harding, G. Erba, G. L. Barkley, and A. Wilkins, "Photic-and pattern-induced seizures: a review for the epilepsy foundation of america working group," Epilepsia, vol. 46, no. 9, pp. 1426–1441, 2005.

[41] M. Jas, D. A. Engemann, Y. Bekhti, F. Raimondo, and A. Gramfort, "Autoreject: Automated artifact rejection for meg and eeg data," NeuroImage, vol. 159, pp. 417–429, 2017.

[42] N. Otsu, "A threshold selection method from gray-level histograms," IEEE transactions on systems, man, and cybernetics, vol. 9, no. 1, pp. 62–66, 1979.

This work is licensed under a Creative Commons Attribution-NonCommercial-NoDerivatives 4.0 License. For more information, see https://creativecommons.org/licenses/by-nc-nd/4.0/

This article has been accepted for publication in IEEE Transactions on Neural Systems and Rehabilitation Engineering. This is the author's version which has not been fully edited and content may change prior to final publication. Citation information: DOI 10.1109/TNSRE.2022.3188184

[43] S. Bhattacharyya, A. Khasnobish, S. Chatterjee, A. Konar, and D. Tibarewala, "Performance analysis of lda, qda and knn algorithms in left-right limb movement classification from eeg data," in 2010 International Conference on Systems in Medicine and Biology, 2010, pp. 126–131.

[44] J. Hu, "Automated detection of driver fatigue based on adaboost classifier with eeg signals," Frontiers in computational neuroscience, vol. 11, p. 72, 2017.

[45] D. R. Edla, K. Mangalorekar, G. Dhavalikar, and S. Dodia, "Classification of eeg data for human mental state analysis using random forest classifier," Procedia computer science, vol. 132, pp. 1523–1532, 2018.

[46] J. Machado, A. Balbinot, and A. Schuck, "A study of the naive bayes classifier for analyzing imaginary movement eeg signals using the periodogram as spectral estimator," in 2013 ISSNIP Biosignals and Biorobotics Conference: Biosignals and Robotics for Better and Safer Living (BRC), 2013, pp. 1–4.

[47] Y.-P. Lin, C.-H. Wang, T.-L. Wu, S.-K. Jeng, and J.-H. Chen, "Multilayer perceptron for eeg signal classification during listening to emotional music," in TENCON 2007 - 2007 IEEE Region 10 Conference, 2007, pp. 1–3.

[48] T. Memmott, A. Koçanaogullari, M. Lawhead, D. Klee, S. Dudy, M. Fried-Oken, and B. Oken, "Bcipy: Brain-computer interface software in python," CoRR, vol. abs/2002.06642, 2020. [Online]. Available: https://arxiv.org/abs/2002.06642

[49] M. Moghadamfalahi, U. Orhan, M. Akcakaya, H. Nezamfar, M. Fried-Oken, and D. Erdogmus, "Language-model assisted brain computer interface for typing: A comparison of matrix and rapid serial visual presentation," IEEE Transactions on Neural Systems and Rehabilitation Engineering, vol. 23, 03 2015.

[50] H. Ramoser, J. Muller-Gerking, and G. Pfurtscheller, "Optimal spatial filtering of single trial eeg during imagined hand movement," IEEE transactions on rehabilitation engineering, vol. 8, no. 4, pp. 441–446, 2000.

[51] J. H. Friedman, "Regularized discriminant analysis," Journal of the American statistical association, vol. 84, no. 405, pp. 165–175, 1989.

[52] M. J. Powell, "An efficient method for finding the minimum of a function of several variables without calculating derivatives," The computer journal, vol. 7, no. 2, pp. 155–162, 1964.

[53] C. R. Harris, K. J. Millman, S. J. van der Walt, R. Gommers, P. Virtanen, D. Cournapeau, E. Wieser, J. Taylor, S. Berg, N. J. Smith et al., "Array programming with numpy," Nature, vol. 585, no. 7825, pp. 357–362, 2020.

[54] F. Pedregosa, G. Varoquaux, A. Gramfort, V. Michel, B. Thirion, O. Grisel, M. Blondel, P. Prettenhofer, R. Weiss, V. Dubourg et al., "Scikit-learn: Machine learning in python," the Journal of machine Learning research, vol. 12, pp. 2825–2830, 2011.

[55] A. Gramfort, M. Luessi, E. Larson, D. A. Engemann, D. Strohmeier, C. Brodbeck, R. Goj, M. Jas, T. Brooks, L. Parkkonen, and M. S. Hämäläinen, "MEG and EEG data analysis with MNE-Python," Frontiers in Neuroscience, vol. 7, no. 267, pp. 1–13, 2013.

[56] L.-M. Vortmann, F. Kroll, and F. Putze, "Eeg-based classification of internally-and externally-directed attention in an augmented reality paradigm," Frontiers in human neuroscience, vol. 13, p. 348, 2019.

[57] C. Bentes, A. R. Peralta, P. Viana, H. Martins, C. Morgado, C. Casimiro, A. C. Franco, A. C. Fonseca, R. Geraldes, P. Canhão et al., "Quantitative eeg and functional outcome following acute ischemic stroke," Clinical Neurophysiology, vol. 129, no. 8, pp. 1680–1687, 2018.

[58] M. Corbetta and G. L. Shulman, "Spatial neglect and attention networks," Annual review of neuroscience, vol. 34, pp. 569–599, 2011.

[59] M. Lunven and P. Bartolomeo, "Attention and spatial cognition: Neural and anatomical substrates of visual neglect," Annals of physical and rehabilitation medicine, vol. 60, no. 3, pp. 124–129, 2017.

[60] J. Driver and J. B. Mattingley, "Parietal neglect and visual awareness," Nature neuroscience, vol. 1, no. 1, pp. 17–22, 1998.

[61] Z. Romeo, D. Mantini, E. Durgoni, L. Passarini, F. Meneghello, and M. Zorzi, "Electrophysiological signatures of resting state networks predict cognitive deficits in stroke," Cortex, vol. 138, pp. 59–71, 2021.

[62] S. Lasaponara, M. Pinto, G. Scozia, M. Pellegrino, M. D'Onofrio, R. Isabella, and F. Doricchi, "Pre-motor deficits in left spatial neglect: An eeg study on contingent negative variation (cnv) and response-related beta oscillatory activity," Neuropsychologia, vol. 147, p. 107572, 2020.

[63] J. J. Foxe and A. C. Snyder, "The role of alpha-band brain oscillations as a sensory suppression mechanism during selective attention," Frontiers in psychology, vol. 2, p. 154, 2011.

[64] M. Bonnefond and O. Jensen, "Alpha oscillations serve to protect working memory maintenance against anticipated distracters," Current biology, vol. 22, no. 20, pp. 1969–1974, 2012.

[65] E. Schleiger, N. Sheikh, T. Rowland, A. Wong, S. Read, and S. Finnigan, "Frontal eeg delta/alpha ratio and screening for post-stroke cognitive deficits: the power of four electrodes," International Journal of Psychophysiology, vol. 94, no. 1, pp. 19–24, 2014.

[66] S. K. Lal and A. Craig, "Driver fatigue: electroencephalography and psychological assessment," Psychophysiology, vol. 39, no. 3, pp. 313–321, 2002.

[67] I. Käthner, S. C. Wriessnegger, G. R. Müller-Putz, A. Kübler, and S. Halder, "Effects of mental workload and fatigue on the p300, alpha and theta band power during operation of an erp (p300) brain–computer interface," Biological psychology, vol. 102, pp. 118–129, 2014.

[68] D. Schneider, A. Göddertz, H. Haase, C. Hickey, and E. Wascher, "Hemispheric asymmetries in eeg alpha oscillations indicate active inhibition during attentional orienting within working memory," Behavioural brain research, vol. 359, pp. 38–46, 2019.

[69] B. I. Hougaard, H. Knoche, J. Jensen, and L. Evald, "Spatial neglect midline diagnostics from virtual reality and eye tracking in a free-viewing environment," Frontiers in Neuroscience, vol. 12, pp. 1–13, 2021.

[70] S. E. Knobel, B. C. Kaufmann, S. M. Gerber, D. Cazzoli, R. M. Müri, T. Nyffeler, and T. Nef, "Immersive 3d virtual reality cancellation task for visual neglect assessment: A pilot study," Frontiers in human neuroscience, vol. 14, p. 180, 2020.

[71] D. Kocanaogullari, J. Mak, J. Kersey, A. Khalaf, S. Ostadabbas, G. Wittenberg, E. Skidmore, and M. Akcakaya, "Eeg-based neglect detection for stroke patients," in 2020 42nd Annual International Conference of the IEEE Engineering in Medicine Biology Society (EMBC), 2020, pp. 264–267.

[72] J. Sarnthein, J. Stern, C. Aufenberg, V. Rousson, and D. Jeanmonod, "Increased eeg power and slowed dominant frequency in patients with neurogenic pain," Brain, vol. 129, no. 1, pp. 55–64, 2006.

[73] B. E. Juel, L. Romundstad, F. Kolstad, J. F. Storm, and P. G. Larsson, "Distinguishing anesthetized from awake state in patients: A new approach using one second segments of raw eeg," Frontiers in human neuroscience, vol. 12, p. 40, 2018.

[74] M. Delazer, M. Sojer, P. Ellmerer, C. Boehme, and T. Benke, "Eye-tracking provides a sensitive measure of exploration deficits after acute right mca stroke," Frontiers in Neurology, vol. 9, 2018.

[75] B. Kortman and K. Nicholls, "Assessing for unilateral spatial neglect using eye-tracking glasses: A feasibility study," Occupational Therapy In Health Care, vol. 30, pp. 1–12, 08 2016.

[76] B. C. Kaufmann, D. Cazzoli, T. Pflugshaupt, S. Bohlhalter, T. Vanbellingen, R. M. Müri, T. Nef, and T. Nyffeler, "Eyetracking during free visual exploration detects neglect more reliably than paper-pencil tests," Cortex, vol. 129, pp. 223–235, 2020.

[77] J. N. Upshaw, D. W. Leitner, B. J. Rutherford, H. B. Miller, and M. R. Libben, "Allocentric versus egocentric neglect in stroke patients: A pilot study investigating the assessment of neglect subtypes and their impacts on functional outcome using eye tracking," Journal of the International Neuropsychological Society, vol. 25, no. 5, pp. 479–489, 2019.

[78] S. Lasaponara, G. Fortunato, D. Conversi, M. Pellegrino, M. Pinto, D. L. Collins, F. Tomaiuolo, and F. Doricchi, "Pupil dilation during orienting of attention and conscious detection of visual targets in patients with left spatial neglect," Cortex, vol. 134, pp. 265–277, 2021.

This work is licensed under a Creative Commons Attribution-NonCommercial-NoDerivatives 4.0 License. For more information, see https://creativecommons.org/licenses/by-nc-nd/4.0/